JCAMECH

Vol. 51, No. 1, June 2020, pp 1-20
DOI: 10.22059/jcamech.2019.272234.350

Torsional wave propagation in 1D and two dimensional functionally graded rod

Alireza Amiri, Hossein Rahmani[a] and Mohammad Ahmadi Balootaki[a]*

[a] *Department of Mechanical Engineering, Shahid Nikbakht faculty, University of Sistan and Baluchestan, Zahedan, Iran*

ARTICLE INFO

Article history:
Received: 24 Deceber 2018
Accepted: 06 May 2019

Keywords:
Functionally graded materials
finite difference method
wave propagation
torsional wave

ABSTRACT

In this study, torsional wave propagation is investigated in a rod that are made of one and two dimensional functionally graded material. Firstly, the governing equations of the wave propagation in the functionally graded cylinder derived in polar coordinate. Secondly, finite difference method is used to discretize the equations. The Von Neumann stability approach is used to obtain the time step size. Two states are assumed for material distribution, in first state it's considered that the material variation occurred only in radial direction (Ti6A14V and Al2O3) and in second state the material properties vary in radial and length directions (BN, Al 1100, Ti6A14V and Al2O3). Moreover, the effect of cutoff frequency and boundary condition in wave propagation is studied. The results were validated by comparing the analytical and numerical solutions for an isotropic rode subjected to a torsional impulsive load. The results show that the torsional wave propagation in FGM rod evidently effects by material composition variation.

1. Introduction

The torsional wave propagates in rotating machines when an unbalancing or unwanted torque is applied. For example, the axels of vehicles or trains in crossing a bump or rotating shafts of helicopters when smashing with a projectile may be affected by a torsional wave. For the first time in the 19th century, the propagation of elastic waves was introduced by Navier. Torsional waves are a type of elastic waves that have been less attention by researchers. The problem of finding torsional vibration responses to structures with circular cross-section was first studied by Pochhammer [1] in 1876 and Chree [2] in 1889. After that, In 1906, Love [3] compiled Pochhammer 's articles on torsional vibration in a summary language. Then the interest in torsional vibrations became an important issue in the field of engineering. The analysis of torsional waves in rotating machine systems is important for the safety and reliability of the system. Excessive torsional vibrations cause severe deformation and even failures. With advances in science and technology, composites were introduced to make parts under mechanical stresses to exhibit better resistance to impact, deformation and failure. But composites are not considered to be a good material against mechanical and thermal stress because of their layered structures. So due to this weakness, new materials were introduced as functionally graded materials. This new materials are a type of composite whose properties are continuously changing [4, 5] . This change in properties according to the designer's requirements can be defined in any direction of material. In the cylindrical bodies, it is usually defined in the radial or axial direction. Due to the unique performance of functionally graded materials in dealing with mechanical and thermal stresses, today they are used in many industries such as nuclear, military, aerospace and automotive [6]. Therefore, due to the increasing use of this type of new material in important industries, the analysis of wave propagation in FG materials is important. While most researchers focus on reducing thermal stress in FG materials, limited studies have been conducted on the propagation of waves in FG materials by analytical and numerical methods.

FG materials have been studied from different view point in science such as thermal, buckling and vibration in mechanical application size and nanotubes [7-17]. Furthermore, in the field of impact and wave stress propagation a lot of researchers pay attention to FGMs. Chio and Erdogan [18] studied the propagation of wave in the FGM plate consisting of SiC and Al. Their simulation was a one-dimensional wave propagation and the properties of plate changed in the direction of thickness. Their work was based on the using Laplace transform technique with various boundary conditions. Shyang-Ho and Yen-Ling [19, 20] obtained the analytical response of the transverse wave propagation by finite element method for the functionally graded plate. Also, the properties of this FG plate are defined by power-law, sigmoid, or exponential functions. Mehmet Dorduncu et al. [21] investigates wave propagation in the functionally graded

* Corresponding author. Tel.: +98-54-31132378; e-mail: H_Rahmani@eng.usb.ac.ir

circular cylinder subjected to dynamic loads. The method used in this study is the finite difference method. The functionally graded cylinder is composed of metal and ceramic, and its properties are defined according to the power-law in the thickness direction. In this work, displacement diagrams, normal stresses and shear stresses have been analyzed for different situations. Elmaimouni et al. [22] devised a different method for investigating the propagation of waves in graded structures. The basis of their method was based on Legendre polynomials and the properties of functionally graded materials are assumed to vary in the direction of the thickness according to a known radial variation law. Assuming the harmonicity of the wave and the use of orthonormality properties, the equation of motion has become an eigenvalue problem. Dorduncu and Apalak [23] studied governing equations of the wave propagation in the functionally graded cylinder by a finite difference method. The top surface of the FG cylinder is pure silicon carbide and the bottom surface is pure aluminum. The material properties vary in the thickness direction and defined by P-FGM power function law. Also, in this study, the volume fractional equations are defined by the Mori-Tanaka scheme. Vollmann et al. [24] examined wave propagation in a two-dimensional functionally graded structure. This FG structure was made of aluminum and gold. The method used to obtain the displacement components of this FG structure was finite difference method. Sun and Leo [25] Used the Hamilton principle and High-order shear deformation plate theory and studied the infinite functionally graded plate subjected to a point impact. Asemi et al. [26] Using Finite element method based on Rayleigh-Ritz energy and studied a cylinder made of functionally graded materials under impact loading. In this study, the stress, natural frequency and displacement are discussed. Shakeri et al. [27] the thick hollow cylinders of FG materials under the axial loading has been investigated. The equations of motion are solved using Galerkin finite element and Newmark methods. Also, the power law functions are used to determine the properties of functionally graded cylinders. Yu et al. [28] studied the wave propagation in a two-dimensional structure of FG material. The method used in this study is an orthogonal polynomial series. The intended structure is a ring with cross-sections that has two type of this ring: Material properties changes in radial direction and material properties changes in axial direction. Stress and displacement profiles are plotted and analyzed for two different modes.

In this paper, the torsional wave propagation in a rod is investigated. The main purpose of doing this research is studying the effect of material distribution with varying properties in torsional wave behavior. For this aim, firstly a long rod is considered and the governing equation of motion in cylindrical coordinate are derived for this rod. The material properties are assumed to be varying in radial direction. In this section, Ti6A14V and Al_2O_3 are considered as composed materials and for different distribution (ceramic rich or metal rich), the stress, strain and displacement of particles are researched.

Secondly, it's supposed the changes of material properties occur in radial and length direction. For this goal, we have two use four material that their dispensation is follow the 2D FGM volume fractions function. BN, Al 1100, Ti6A14V and Al_2O_3 (two ceramic and two metal) are the materials that chosen. In this section, the influence of permutation of material in elastic behavior of rod (stress, strain and displacement) and wave propagation are studied.

The main novelty of this research is studying the torsional wave propagation in FGM rod. As mentioned later, it can be used practically in manufacturing of axels of trains or vehicles and also other rotating shafts in centrifuges of nuclear applications, power plants, helicopters and aerospace industry and military devices. By using FGM rods and shafts, we can guide the stress waves to the favorite part of rod and reduce the risk of failure.

2. Basic equation

Functionally graded materials, due to their properties, can reduce the mechanical and thermal stresses of structures. So the properties of these materials are very important. In the following, we explain the distribution of properties of the FG rod in one-dimensional and two-dimensional states.

2.1. One-Dimensional FG rod

A functionally graded rod with a radius R is considered. It is assumed that the changes in the properties of the desired rod in the direction of radial occurred. The materials intended for this rod are ceramic and metal. In the distance between the center of the rod and the external surface of the FG rod (rod radius), the properties are determined according to the following equation [24]:

$$P = \left(P_m - P_c\right)\left(\frac{R-r}{R}\right)^n + P_c \tag{1}$$

which P can be any material properties such as density, young modulus, and etc. The volume fraction of the material, n is also non-negative. Subscript m and c related to ceramics and metal.

As is clear from Equation (1) when $r = R$, the properties of the FG rod are equal to the pure ceramic properties, that's mean $P = P_c$ and when $r = 0$, the properties of the FG rod are equal to the properties of the pure metal, that's mean $P = P_m$.

2.2. Tow-Dimensional FG rod

The two-dimensional FG rod discussed in this study consists of several gradient phases. This means that the functionally graded rod consists of 4 different materials, as shown in Figure 1, the two ceramics used in this rod (c_1 and c_2) and the other two metals are (m_1 and m_2). Due to the volume fractions defined for this functionally graded rod, material properties are defined in two dimensions and V_{c1} ، V_{c2} ، V_{m1} و V_{m2} denote volume fractions of the first ceramic, second ceramic, first metal and the second metal ,respectively.

Due to the distribution of properties of materials in Fig. 1, the volume fraction of each of the elements used in the FG rod can be obtained from the following relationship [29]:

$$V_{m1}(r,z) = \left[1-\left(\frac{r}{R}\right)^{n_r}\right]\left[1-\left(\frac{z}{L}\right)^{n_z}\right]$$

$$V_{m2}(r,z) = \left[\left(\frac{r}{R}\right)^{n_r}\right]\left[\left(\frac{z}{L}\right)^{n_z}\right]$$

$$V_{c1}(r,z)=\left[1-\left(\frac{r}{R}\right)^{n_r}\right]\left[\left(\frac{z}{L}\right)^{n_z}\right]$$
$$V_{c2}(r,z)=\left[\left(\frac{r}{R}\right)^{n_r}\right]\left[1-\left(\frac{z}{L}\right)^{n_z}\right] \quad (2)$$

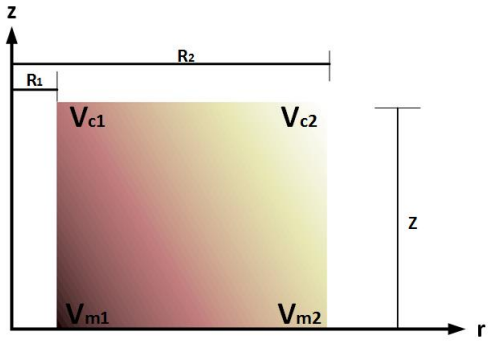

Figure 1. Functionally graded rod composed of four different materials

For the use of volume fractions, the following rules should be observed [30]:

2.2.1. First rule

The sum of all fractions of volumes should be equal to one, that is:

$$Vc_1+Vc_2+Vm_1+Vm_2=1 \quad (3)$$

2.2.2. Second rule

The maximum value of each volume fraction must not exceed one and the minimum value must not be less than zero, that is:

$$\begin{aligned}&0\le Vc_1\le 1\\&0\le Vc_2\le 1\\&0\le Vm_1\le 1\\&0\le Vm_2\le 1\end{aligned} \quad (4)$$

2.3. Equations of motion

The cylindrical coordinate system (r,z,θ) is assumed to simulate the stress wave propagation in FG rod. The equations of motion in terms of stress components are given by [31]:

$$\frac{\partial T_{rr}}{\partial r}+\frac{\partial T_{rz}}{\partial z}+\frac{1}{r}\frac{\partial T_{r\theta}}{\partial \theta}+\frac{T_{rr}-T_{\theta\theta}}{r}=\rho\frac{\partial^2 u}{\partial t^2} \quad (5)$$

$$\frac{1}{r}\frac{\partial T_{\theta\theta}}{\partial \theta}+\frac{\partial T_{\theta z}}{\partial z}+\frac{\partial T_{r\theta}}{\partial r}+\frac{2T_{r\theta}}{r}=\rho\frac{\partial^2 v}{\partial t^2} \quad (6)$$

$$\frac{\partial T_{zz}}{\partial z}+\frac{1}{r}\frac{\partial T_{\theta z}}{\partial \theta}+\frac{\partial T_{rz}}{\partial r}+\frac{T_{rz}}{r}=\rho\frac{\partial^2 w}{\partial t^2} \quad (7)$$

Equations (5) to (7) be called equations of motion in 3D cylindrical coordinates, also known as Navier's equations. u, v, w are radial, angular and axial displacements, Respectively.

So, the rod is defined by the following equation:

$$\begin{aligned}&0<r<R\\&0<\theta<2\pi\\&0<z<Z\end{aligned} \quad (8)$$

The components of stress in terms of displacement are written as follows [31]:

$$\begin{aligned}T_{rr}&=(\lambda+2\mu)\left(\frac{\partial u}{\partial r}\right)+\lambda\left(\frac{1}{r}\frac{\partial v}{\partial \theta}+\frac{u}{r}+\frac{\partial w}{\partial z}\right)\\T_{\theta\theta}&=(\lambda+2\mu)\left(\frac{1}{r}\frac{\partial v}{\partial \theta}+\frac{u}{r}\right)+\lambda\left(\frac{\partial u}{\partial r}+\frac{\partial w}{\partial z}\right)\\T_{zz}&=(\lambda+2\mu)\left(\frac{\partial w}{\partial z}\right)+\lambda\left(\frac{\partial u}{\partial r}+\frac{1}{r}\frac{\partial v}{\partial \theta}+\frac{u}{r}\right)\\T_{r\theta}&=\mu\left(\frac{\partial v}{\partial r}-\frac{v}{r}+\frac{1}{r}\frac{\partial u}{\partial \theta}\right)\\T_{z\theta}&=\mu\left(\frac{\partial v}{\partial z}-\frac{v}{r}+\frac{1}{r}\frac{\partial w}{\partial \theta}\right)\\T_{rz}&=\mu\left(\frac{\partial u}{\partial z}+\frac{\partial w}{\partial r}\right)\end{aligned} \quad (9)$$

The properties of the elastic medium are given by the two Lamé constants $\lambda=\lambda(z)$ and $\mu=\mu(z)$.

Now, Substituting Eq. (9) into equations (5) to (7) yields

$$\begin{aligned}\rho\frac{\partial^2 u}{\partial t^2}=&-(\lambda+2\mu)\frac{u}{r^2}+\mu\frac{\partial^2 u}{\partial z^2}-(\lambda+3\mu)\frac{1}{r^2}\frac{\partial v}{\partial \theta}\\&+\mu\frac{1}{r^2}\frac{\partial^2 u}{\partial \theta^2}+(\lambda+2\mu)\frac{1}{r}\frac{\partial u}{\partial r}\\&+(\lambda+\mu)\frac{\partial^2 w}{\partial r\partial z}+(\lambda+\mu)\frac{1}{r}\frac{\partial^2 v}{\partial r\partial \theta}\\&+(\lambda+2\mu)\frac{\partial^2 u}{\partial r^2}\end{aligned} \quad (10)$$

$$\begin{aligned}\rho\frac{\partial^2 v}{\partial t^2}=&-\mu\frac{1}{r^2}v+\mu\frac{\partial^2 v}{\partial z^2}+(\lambda+3\mu)\frac{1}{r^2}\frac{\partial u}{\partial \theta}\\&+(\lambda+\mu)\frac{1}{r}\frac{\partial^2 w}{\partial \theta\partial z}+(\lambda+2\mu)\frac{1}{r^2}\frac{\partial^2 v}{\partial \theta^2}\\&+\mu\frac{1}{r}\frac{\partial v}{\partial r}+(\lambda+\mu)\frac{1}{r}\frac{\partial^2 u}{\partial r\partial \theta}+\mu\frac{\partial^2 v}{\partial r^2}\end{aligned} \quad (11)$$

$$\begin{aligned}\rho\frac{\partial^2 w}{\partial t^2}=&(\lambda+\mu)\frac{1}{r}\frac{\partial u}{\partial z}+(\lambda+2\mu)\frac{\partial^2 w}{\partial z^2}\\&+(\lambda+\mu)\frac{1}{r}\frac{\partial^2 v}{\partial \theta\partial z}+\mu\frac{1}{r^2}\frac{\partial^2 w}{\partial \theta^2}\\&+\mu\frac{1}{r}\frac{\partial w}{\partial r}+(\lambda+\mu)\frac{\partial^2 u}{\partial r\partial z}+\mu\frac{\partial^2 w}{\partial r^2}\end{aligned} \quad (12)$$

For a torsional wave, according to the symmetry characteristics, radial, angular and axial displacement vectors are defined as follows [32].

$$u = 0,$$
$$v = v(r, z, t), \qquad (13)$$
$$w = 0$$

Therefore, only the nonzero equation of motion, regardless of the body forces, is obtained for the torsion wave as follows:

$$\rho \frac{\partial^2 v}{\partial t^2} = -\mu \frac{1}{r^2} v + \mu \frac{\partial^2 v}{\partial z^2} + \mu \frac{1}{r} \frac{\partial v}{\partial r} + \mu \frac{\partial^2 v}{\partial r^2} \qquad (14)$$

The Von Neumman stability criterion is used to determine the time step size as follow[26]:

$$\Delta t \le \frac{\Delta r}{\sqrt{\frac{5}{4} + q^2 \left(\frac{\Delta r}{\Delta z} \right)^2}} \quad and \quad \frac{\Delta t}{\Delta z} \le 1$$

Where q is the ratio of shear stress wave velocity to longitudinal stress wave propagation velocity in material.

2.4. Boundary condition and initial condition

At t = 0, the following initial conditions are considered:

It is assumed that at the instant t = 0 there is no stress in the FG rod, so:

$$T_{r\theta} = T_{z\theta} = 0 \qquad (15)$$

It is also assumed at this moment there is no displacement in functionally graded rod:

$$v(r, z, t) = 0 \qquad (16)$$

The governing boundary conditions on the problem are also assumed:

$$T_{z\theta} = M \qquad (Z = 0)$$
$$T_{r\theta} = 0 \qquad (r = R) \qquad (17)$$

In the previous equation, M is defined as:

$$M = M_0 \left[H(t) - H(t - t_0) \right] \qquad (18)$$

The applied load on the FG rod as a pulse is shown in Fig. 2:

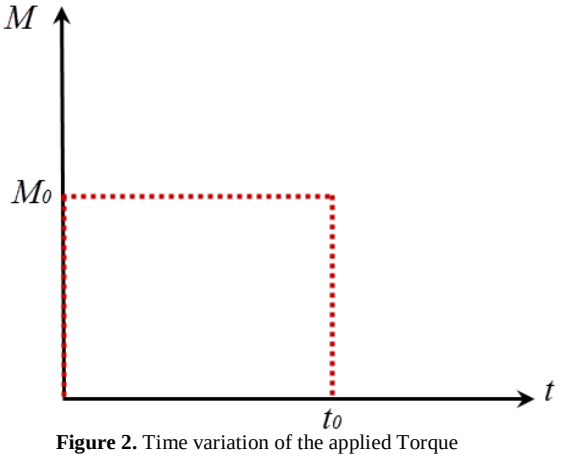

Figure 2. Time variation of the applied Torque

Which the value of t_0 is 40 microseconds and M_0 is equal to 1000 Newton meters. Also $H(t)$ is a Heaviside function.

3. Finite difference implementation

This method is based on the Taylor expansion and the simple application of derivative definition. In short, in explaining this method, the space studied is completely networked with equal distances. After that, all space is introduced by the points created. Then, by introducing boundary conditions and initial conditions, properties of all points will be obtained. In general, there are two explicit and implicit methods for solving differential equations using finite difference methods. In the explicit method, using the data of the previous points in the grid, the properties of next points are calculated, but in the implicit method, the equations for the past and future times are solved in order to calculate the data of the present. In order to solve the wave equation in this research, the explicit method of central differential approximation is used.

3.1. Approximation of the central difference method

First, we make the following important statement about the derivatives of partial differential equations:

Derivatives in the partial differential equation are approximated using the linear combination of function values in the network points.

Figure 3. A domain grid for specific interval 0 to X

Using derivative fundamental definition and according to Fig. 3, the first derivative of the first order for the hypothesized function is computed as follows:

$$\frac{\partial u}{\partial x}(\bar{x}) = \lim_{\Delta x \to 0} \frac{u(\bar{x} + \Delta x) - u(\bar{x})}{\Delta x} = \lim_{\Delta x \to 0} \frac{u(\bar{x}) - u(\bar{x} - \Delta x)}{\Delta x} = \lim_{\Delta x \to 0} \frac{u(\bar{x} + \Delta x) - u(\bar{x} - \Delta x)}{2\Delta x} \qquad (19)$$

Using the definition of Eq. (19) for the second-order derivative, we have:

$$\frac{\partial^2 u}{\partial x^2} = \left[\frac{\partial}{\partial x} \left(\frac{\partial u}{\partial x} \right) \right] = \lim_{\Delta x \to 0} \frac{\frac{u_{i+1} - u_i}{\Delta x} - \frac{u_i - u_{i-1}}{\Delta x}}{\Delta x} = \lim_{\Delta x \to 0} \frac{u_{i+1} - 2u_i + u_{i-1}}{(\Delta x)^2} \qquad (20)$$

Equations (19) and (20) are calculated for the hypothesized function $u(x_i)$ and to the hypothetical point. Therefore, since in the finite difference method, the time interval is also regular networking, the time derivative of the desired function can be calculated in the same way.

The centered-difference equations of the second-order derivatives of a displacement component, such as $v(r, z, t)$ at the nodal (i, j) with respect to time t is given by [33]

$$\frac{\partial^2 v}{\partial t^2}=\frac{v_{i,j}^{k+1}-2v_{i,j}^{k}+v_{i,j}^{k-1}}{\left(\Delta t\right)^2} \tag{21}$$

Δt the size of the time interval, k refers to the time index and i, j the position of the points in the network are indicated.

The finite difference equations of the first- and second-order derivatives of the displacement component $v(r,z,t)$ at the node (i, j) with respect to the spatial variables r and z are shown in Eq. (22):

$$\begin{aligned}
&\frac{\partial v}{\partial r}=\frac{v_{i+1,j}^{k}-v_{i-1,j}^{k}}{2\Delta r}\\
&\frac{\partial v}{\partial z}=\frac{v_{i,j+1}^{k}-v_{i,j-1}^{k}}{2\Delta z}\\
&\frac{\partial^2 v}{\partial r^2}=\frac{v_{i+1,j}^{k}-2v_{i,j}^{k}+v_{i-1,j}^{k}}{\left(\Delta r\right)^2}\\
&\frac{\partial^2 v}{\partial z^2}=\frac{v_{i,j+1}^{k}-2v_{i,j}^{k}+v_{i,j-1}^{k}}{\left(\Delta z\right)^2}
\end{aligned} \tag{22}$$

By placing the equations (21) and (22) in equation (14), the equation of 2-D torsional wave propagation in functionally graded rod in the case of finite difference equation obtained

$$\begin{aligned}
\rho\frac{v_{i,j}^{k+1}-2v_{i,j}^{k}+v_{i,j}^{k-1}}{\left(\Delta t\right)^2}=&-\mu\left(\frac{v_{i,j}^{k}}{\left(idr\right)^2}\right)+\mu\left(\frac{v_{i,j+1}^{k}-2v_{i,j}^{k}+v_{i,j-1}^{k}}{\left(\Delta z\right)^2}\right)\\
&+\mu\left(\frac{1}{\left(idr\right)}\right)\left(\frac{v_{i+1,j}^{k}-v_{i-1,j}^{k}}{2\Delta r}\right)+\mu\left(\frac{v_{i+1,j}^{k}-2v_{i,j}^{k}+v_{i-1,j}^{k}}{\left(\Delta r\right)^2}\right)
\end{aligned} \tag{23}$$

4. Problem description

To study the torsional wave propagation relations in a circular rod made of functionally graded material, hollow cylindrical cross-sectional are considered. The cylindrical coordinates including r in the radial direction, θ in the angular direction, and z in the longitudinal direction of the cylinder are shown in Fig. 4.

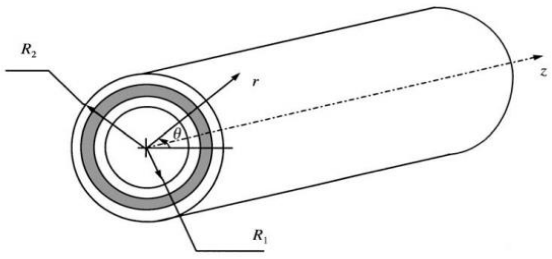

Figure 4. The structure of the FG rod

Since the condition of the equations is axial symmetry, we will separate and distinguish the specified ABCD page in Fig. 5. Obviously, all conditions in this case are symmetrical to the central axis. In Fig. 5, the page along with the points M, N, P and Q that are shown for the getting data and comparison of the results.

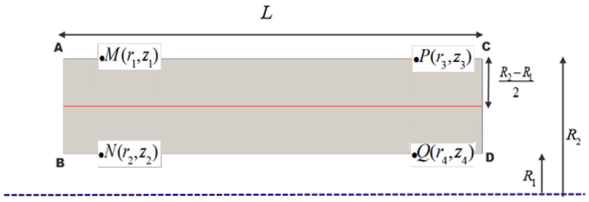

Figure 5. Selected points for the getting data in the FG rod

This rod is being tested under various states in order to ensure the accuracy of the results obtained.

4.1. State 1

In the first state, in order to ensure the accuracy of the results, it is assumed that the rod is composed of an isotropic material. The isotropic conditions in the material are obtained by setting the value n = 0 in Eq. (1).

In this case, the dimension of the rod and the problem conditions is considered as shown in Table 1.

Table 1. Dimension and the problem condition of the rod in state 1

	t_0(s)	T(s)	M_0(N.m)	R_2(mm)	R_1(mm)	L(mm)
State1	40	300	1000	15	5	150

The material used in this case is Ti6A14V, which is due to the insertion of a zero value in the Eq. (1), the desired rod is assumed to be isotropic. Then, the results obtained from the governing equations by the finite difference method that will be compared with the analytical results of a one-dimensional wave propagation.

The mechanical properties of the Ti6A14V are as follows:

Table 2. Properties of Ti6A14V

Material	E (Gpa)	$\rho(\frac{kg}{m^3})$	ϑ
Ti6A14V	120	4515	0.31

The coordinates of the M, N, P, and Q points that are selected for the getting data in this state are as follows:

Table 3. Selected points for the getting data in state 1

	M	N	P	Q
R(mm)	15	5	15	5
Z(mm)	10	10	140	140

4.2. State 2

In this state, it is assumed that the change of properties occurs only in the direction of radius. As a result, the functionally graded rod is composed of two different materials, the inner part being pure from material 1 and the outer part is pure from material 2, so changing properties occurs in the radial direction. Changing Properties for different values of n are considered to be 1 (linear mode), 0.1 and 10. The dimensions, applied torque, pulse time and the coordinates of the data points are considered similar to the first one, as shown in Tables 1 and 3. The properties of the materials used in this case are given in the following Table 4.

Table 4. Material properties in state 2

Constituents	Material	E (Gpa)	$\rho(\frac{kg}{m^3})$	ϑ
m_2	Ti6A14V	120	4515	0.31
c_1	Al2O3	150	3470	0.21

It should be noted that the changes in this state for the first specimen, assuming that the inner part of the rod is from the metal and the outer part of the ceramic, and then for the second specimen, assuming that the inner part of the ceramic and the outer part of the metal be studied.

4.3. State 3

In the third state it is assumed that the changing properties occur both in the radial direction and in the longitudinal direction. In this case, the dimension of the rode is as follows:

Table 5. Dimension and the problem condition of the rod in state 3

	t_0(s)	T(μs)	M_0(N.m)	R_2(mm)	R_1(mm)	L(mm)
State 3	40	100	1000	50	10	150

The coordinates of the M, N, P, and Q points that are selected for the getting data in this state are as follows:

Table 6. Selected points for the getting data in state 3

	M	N	P	Q
R(mm)	50	10	50	10
Z(mm)	10	10	90	90

The properties of materials used to model two-dimensional FGM rod are given in the following table:

Table 7. Material properties in state 3

Constituents	Material	E (Gpa)	$\rho(\frac{kg}{m^3})$	ϑ
m_1	Al 1100	75	2715	0.33
m_2	Ti6A14V	120	4515	0.31
c_2	BN	675	2100	0.27
c_1	Al2O3	150	3470	0.21

The distribution of materials according to the naming in the Figure 5 is shown in the table 8:

Table 8. Distribution of materials for four different Model

	Point A	Point B	Point C	Point D
Model 1	C_1	M_1	C_2	M_2
Model 2	M_1	C_1	M_2	C_2
Model 3	C_2	M_2	C_1	M_1
Model 4	M_2	C_2	M_1	C_1

It should be noted that in the above table, the equations are considered only for the n = 1 (linear distribution).

5. Numerical result

5.1. State 1: isotropic rod

According to the torsion theory, it is expected that the stress and strain in the $\sigma_{rr},\sigma_{r\theta},\sigma_{rz},\sigma_{\theta\theta},\sigma_{zz}$ and $\varepsilon_{rr},\varepsilon_{r\theta},\varepsilon_{rz},\varepsilon_{\theta\theta},\varepsilon_{zz}$ directions are equal to zero and only the non-zero stress and non-zero strain will occur in the $z\theta$ direction. As shown in Fig. 6 and 7, the stresses $\sigma_{rr},\sigma_{r\theta},\sigma_{rz},\sigma_{\theta\theta},\sigma_{zz}$ are negligible than stress. In Fig. 6, considering the properties of the material as a change in one dimension, the maximum stress value associated with the point P on the outer radius and the lowest stress in this case, occurred in the point N, which is on the inner radius. In order to ensure the obtained equations and Figures, the stress values at M, N, P, and Q points are calculated using the one-dimensional wave theory, which is analyzed analytically by the d'Alembert method in [34] ,and with the results obtained in this research is compared in Fig. 8.

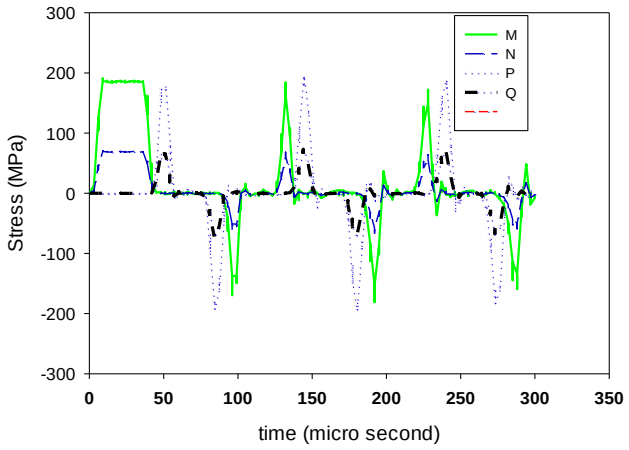

Figure 6. Distributions of the shear stress component, $\sigma_{z\theta}$ In terms of time for the points M, N, P and Q in isotropic mode

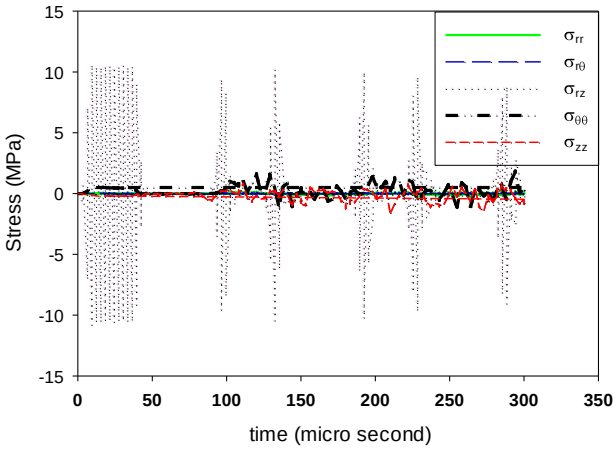

(a)

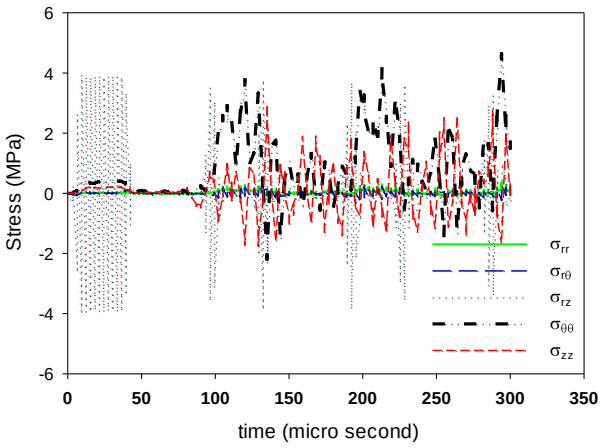

(b)

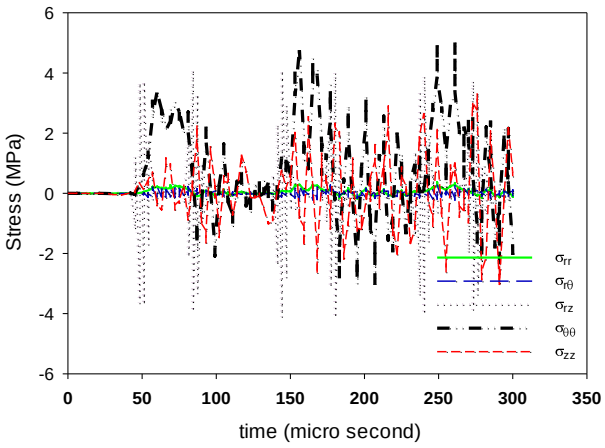

(d)

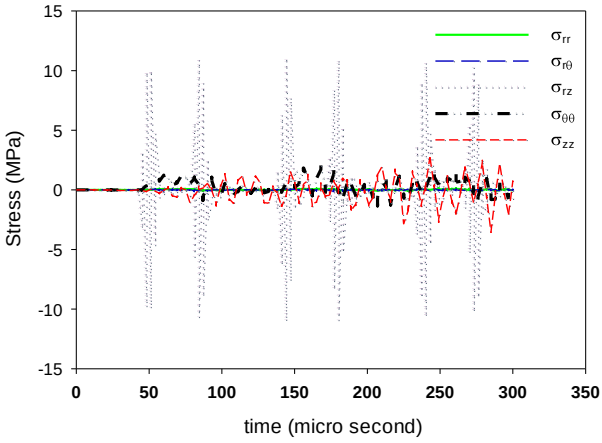

(c)

Figure 7. Distributions of the stress components $\sigma_{rr}, \sigma_{r\theta}, \sigma_{rz}, \sigma_{\theta\theta}, \sigma_{zz}$ In terms of time for the points (a)M, (b)N, (c)P, (d)Q in isotropic mode

As expected, at M and P points, the stress values are larger than N and Q, and there is also a good fit between the results in terms of validation. Regarding the interference of propagated waves and the complexity of the analytic equations, numerical and analytical results are compared with once the wave flux. In this case, the wave completely passes through the points M and N, and after the wave reaches the end of the rod, the return wave goes back into the rod and causes the wave pulse to be shortened at points P and Q, because Due to the proximity of the points above to the end of the rod, moments after passing the passing wave, the return wave reaches the desired points and neutralizes the stresses. The strain values in this study are directly related to stress values and have similar behavior to stress behavior.

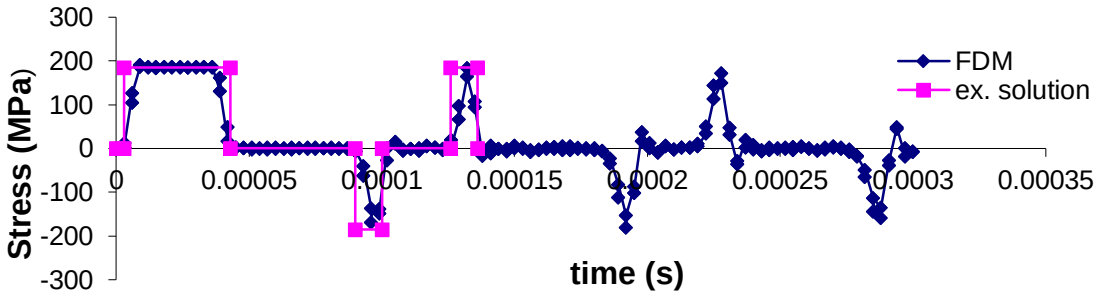

(a)

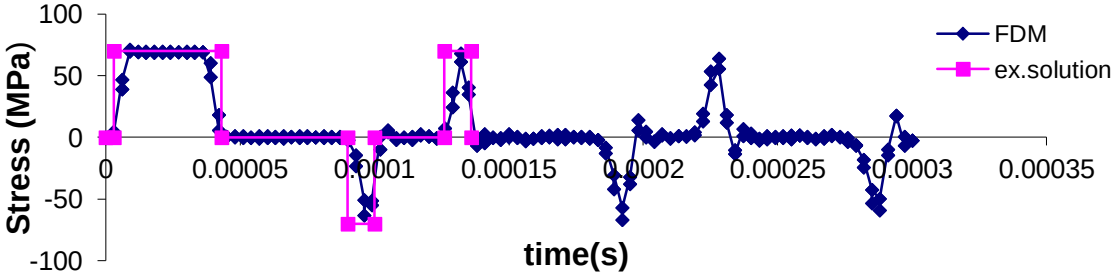

(b)

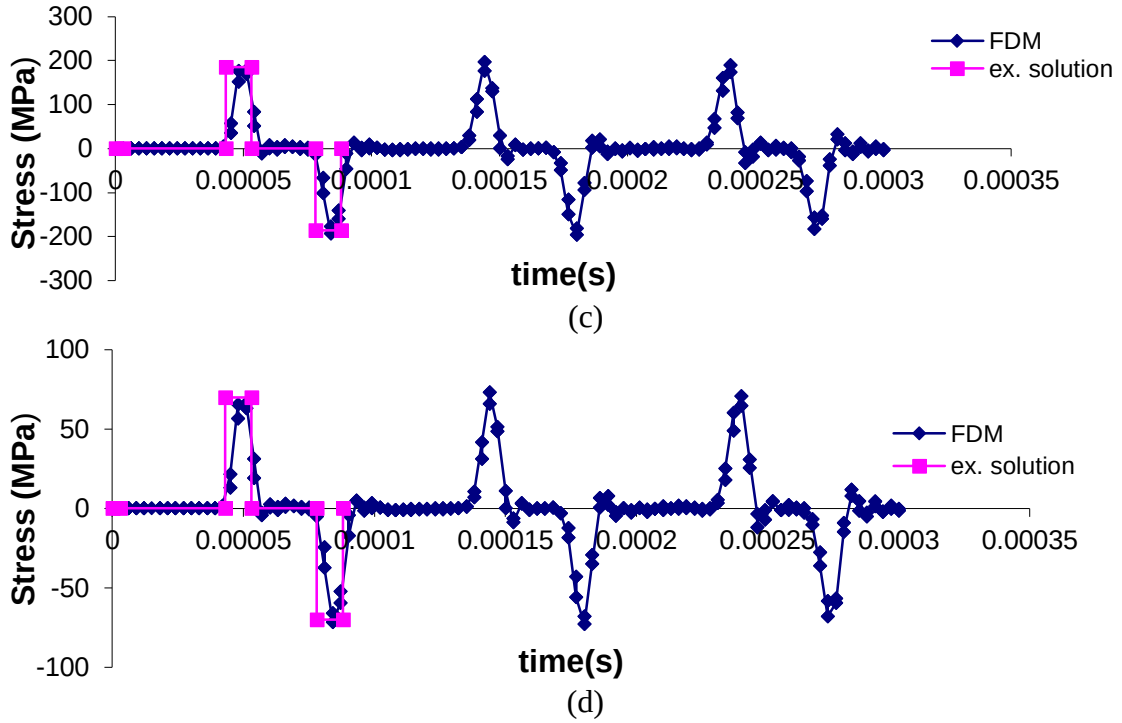

Figure 8. Validation of stress value at points (a)M, (b)N, (c)P, (d)Q for isotropic rod

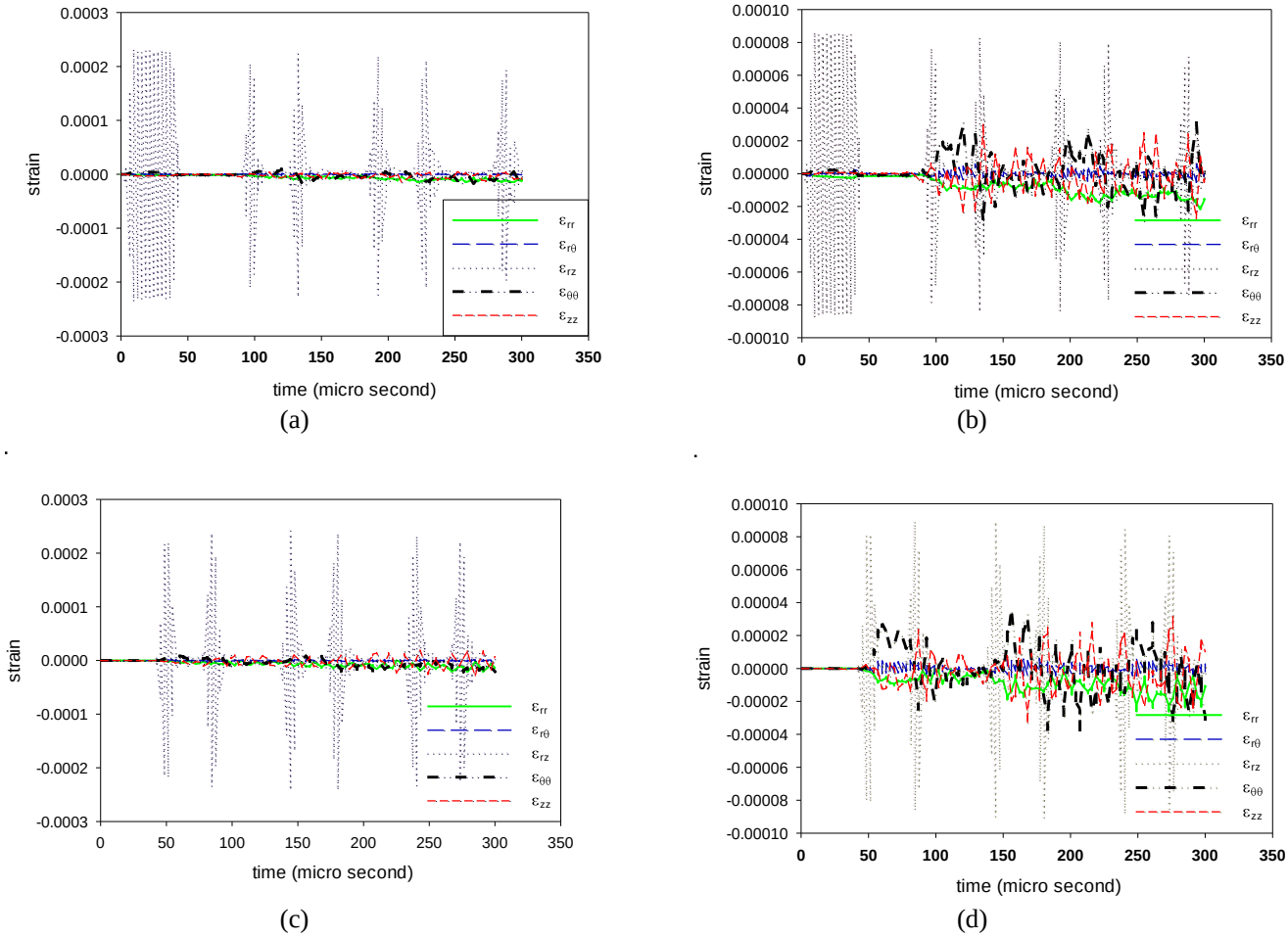

Figure 9. Distributions of the strain components $\varepsilon_{rr}, \varepsilon_{r\theta}, \varepsilon_{rz}, \varepsilon_{\theta\theta}, \varepsilon_{zz}$ In terms of time for the points (a)M, (b)N, (c)P, (d)Q in isotropic mode

As shown in Figures 9 and 10, the strain values $\varepsilon_{rr}, \varepsilon_{r\theta}, \varepsilon_{rz}, \varepsilon_{\theta\theta}, \varepsilon_{zz}$ are much less than $\varepsilon_{z\theta}$. In this case, in Fig. 10, the maximum strain value at the point P and the lowest strain value occurred at the point N. As it was proved in the previous chapter, it is expected that the amount of radial displacement in most other directions, or in other words, in non-radial directions, has a zero-displacement value, but due to computational errors, as well As seen from Fig. 11, the displacement values in r and z are non-zero. However, in comparison with the amount of displacement in radial direction, they are smaller and can be neglected. Fig. 11 shows the displacement-time diagrams in isotropic rode.

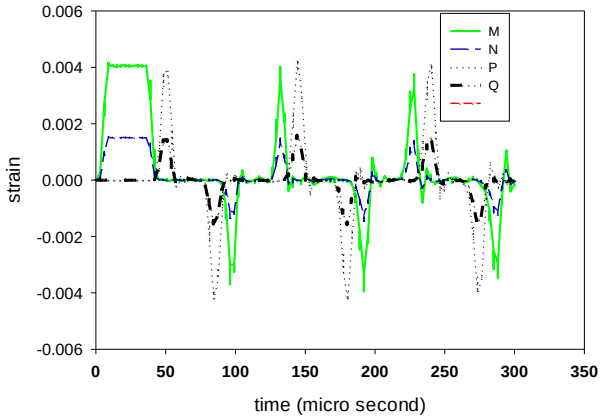

Figure 10. Distributions of the shear strain component, $\varepsilon_{z\theta}$ In terms of time for the points M, N, P and Q in isotropic mode

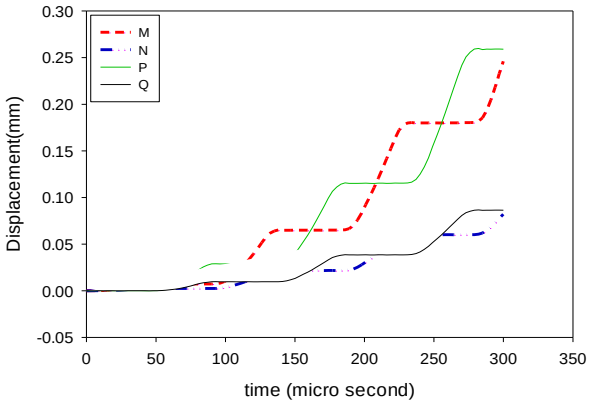

(a)

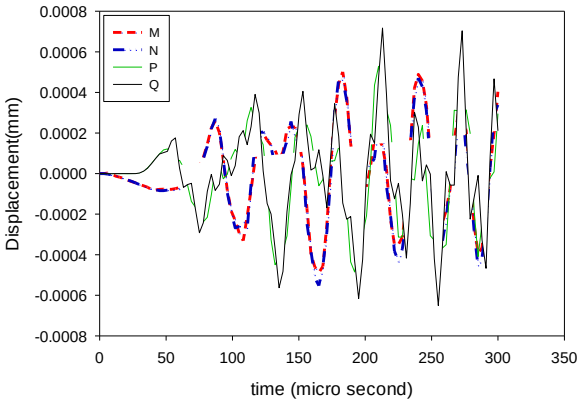

(c)

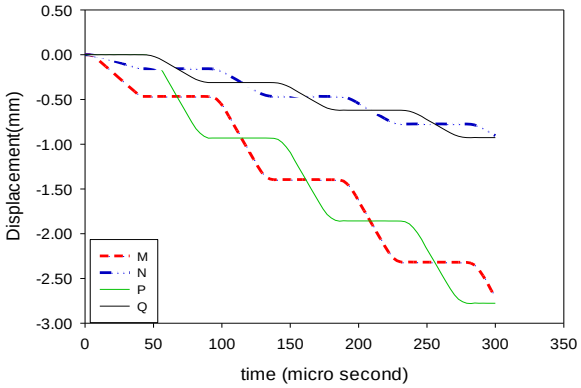

(b)

Figure 11. Distributions of the displacement components (a) u ,(b) v ,(c) w In terms of time for the points M, N, P and Q in isotropic mode

As shown in Fig. 11, the maximum displacement value is initially related to the v displacement chart, then u and w displacements chart, respectively.

Note: Due to the fact that the stresses $\sigma_{rr}, \sigma_{r\theta}, \sigma_{rz}, \sigma_{\theta\theta}, \sigma_{zz}$ and strains $\varepsilon_{rr}, \varepsilon_{r\theta}, \varepsilon_{rz}, \varepsilon_{\theta\theta}, \varepsilon_{zz}$ are very smaller than $\sigma_{\theta z}$ and $\varepsilon_{\theta z}$, so they are neglected and in the following, they have been discarded.

5.2. State 2: FGM rod with one-dimensional distribution of materials

As already mentioned, the 2nd state is divided into two parts: the first specimen, assuming that the inner part of the FG rod is of metal and the outer part of the ceramic, and then the second specimen, assuming that the inner part of the ceramic and the outer part of the Metal is considered.

5.2.1. First specimen

In this case, the inner part of FG rod is made of Ti6A14V and the outer part of the Al2O3. To analyze this specimen, three modes have been used:

When $n=1$: In this mode, the internal part of the Ti6A14V and the outer part of Al2O3 are actually formed and the properties in the radial direction are changed linearly.

When $n=0.1$: In this mode, the internal part of Ti6A14V and the outer part of Al2O3, but the changing properties are such that within a short distance from the inner radius, Ti6A14V is rapidly reduced and most parts of the rode composed form Al2O3, actually.

When $n=10$: The structure of the rod in this mode is the same as in the previous two modes, but the changes in properties are such that at a short distance from the outer radius of the rod, the Al2O3 value decreases rapidly, and the dominant part of the rod is displaced by Ti6A14V.

The following Figure of stress variations in time are given for this specimen:

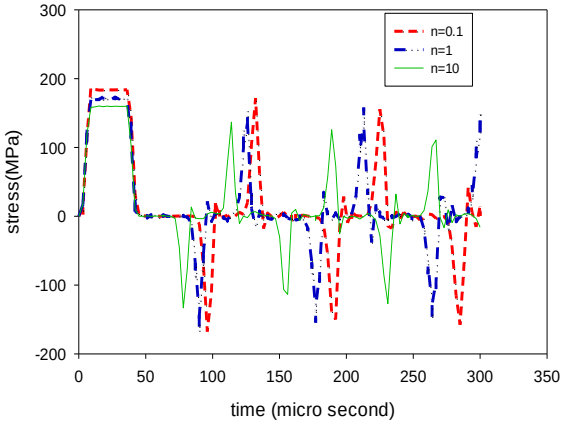

(a)

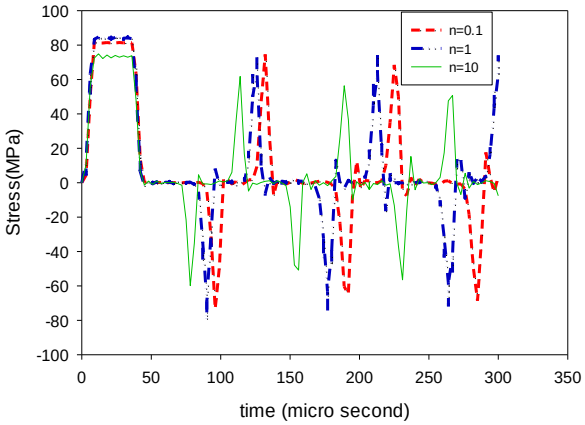

(b)

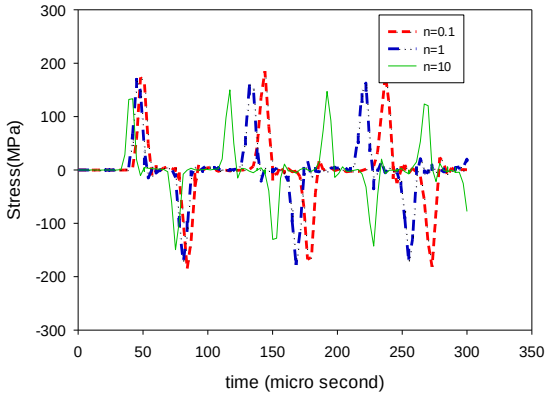

(c)

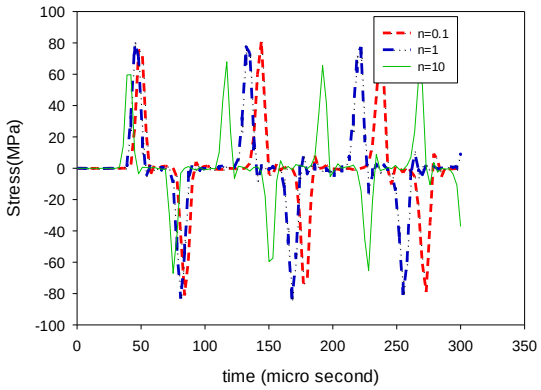

(d)

Figure 12. Distributions of the shear stress component $\sigma_{\theta z}$ In terms of time for the points (a)M,(b) N,(c) P and (d)Q for the compositional gradient exponents $n = 0.1,1,10$ for first specimen

As shown in Fig. 12, the maximum stress value in this case is related to points M and P, and the lowest stress are related to points N and Q. Also, in all points, the maximum stress is in the mode $n=0.1$ and the least stress is in the mode $n=10$. Another noteworthy point is that, since in state 2, the changing of the properties have been taken in the form of a one dimensional and in radial direction, it can be said that the variation of stress in points that are located on the same radius is approximately equal, then the points M And P, as well as the two point N and Q that are on a radius, will experience almost identical variations in this state.

Also, as shown in Figure 13, the strain variation in time charts are plotted for the first specimen for three modes, separated by four points M, N, P and Q:

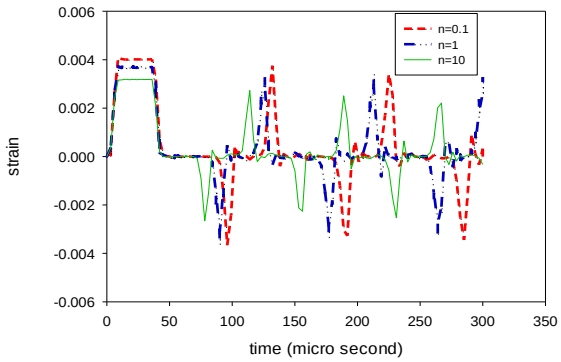

(a)

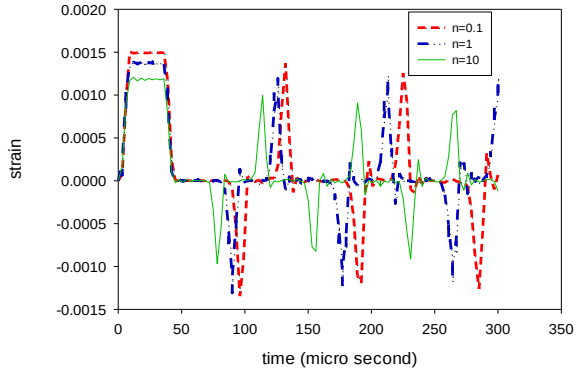

(b)

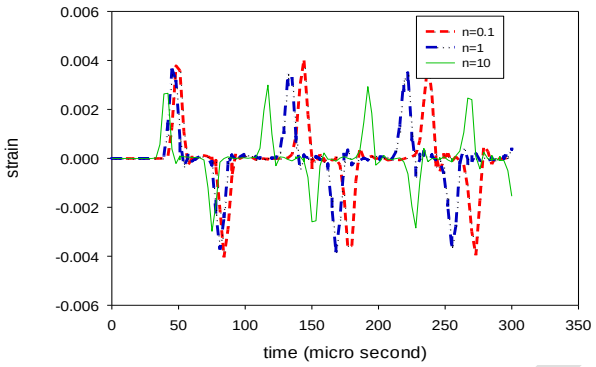

(c)

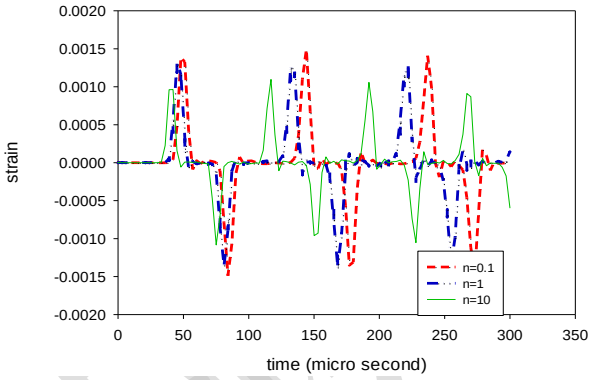

(d)

Figure 13. Distributions of the shear strain component $\varepsilon_{\theta z}$ In terms of time for the points (a)M,(b) N,(c) P and (d)Q for the compositional gradient exponents $n = 0.1,1,10$ for first specimen

Since strain values are directly related to stress values in this study, in the strain variation charts, the maximum strain values are related to the points M and P. also due to the unidirectional changes in rod properties, these two points experience the same variation of strain in this case. On the other hand, the points N and Q also have roughly identical variations in the strain values in this case. In all four points, the highest rate of strain variation is related to the $n = 0.1$ and the lowest rate of change is also related to the $n = 10$.

In the following, displacement variation in time charts are plotted for $n = 0.1,1,10$, separated by points M, N, P, and Q.

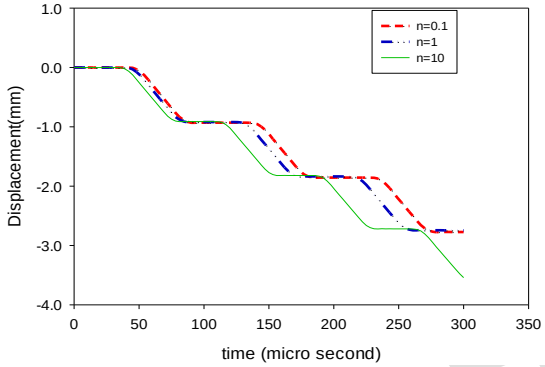

(a)

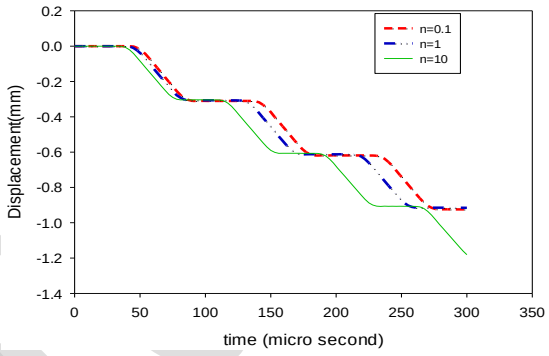

(b)

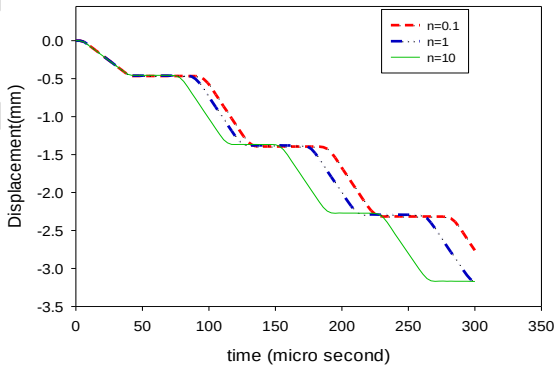

(c)

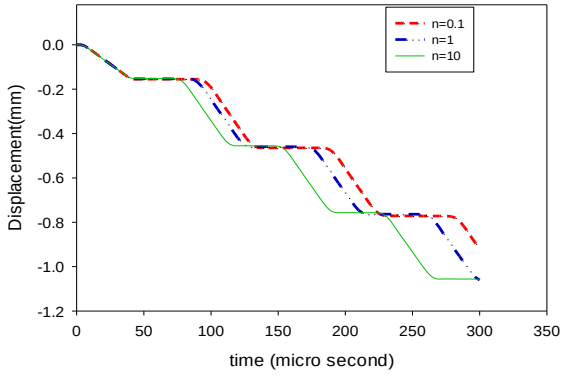

(d)

Figure 14. Distributions of the displacement component v In terms of time for the points (a)M,(b) N,(c) P and (d)Q for the compositional gradient exponents $n = 0.1,1,10$ for first specimen

In Fig. 14, the maximum value of displacement relative to the points M and P is 3 millimeter and the minimum value of

displacement is related to the points N and Q is approximately 1.2 millimeter. Another point is that the displacement chart has almost the same behavior at all four points.

5.2.2. Second specimen

In the second specimen, as in the first specimen, the FG rod is made of two materials of ceramic and metal, and the changes of properties are in one direction. In this case, the inner part of the FG rod is made of Al2O3 and the outer part of the Ti6A14V. For analysis of the second specimen, the following three modes are used:

When $n=1$: In this mode, the inside of the functionally graded rod is made of Al2O3 and the external part of FG rod compose of the Ti6A14V. Also, the changing properties will be linear.

When $n=0.1$: In this case, the internal and external portions of the FG rod are composed of Al2O3 and Ti6A14V, respectively. The changes in properties are such that, at a short distance from the internal radius, the amount of Al2O3 decreases and most of the properties of material are dedicated to the Ti6A14V.

When $n=10$: This mode like the two previous modes, consists of both Al2O3 and Ti6A14V for the internal and external sections of the FG rod, respectively. Also, the dominant part of the rod in this section is Al2O3. Stress variation charts are plotted in time for the second specimen for three modes, separated by four points M, N, P and Q:

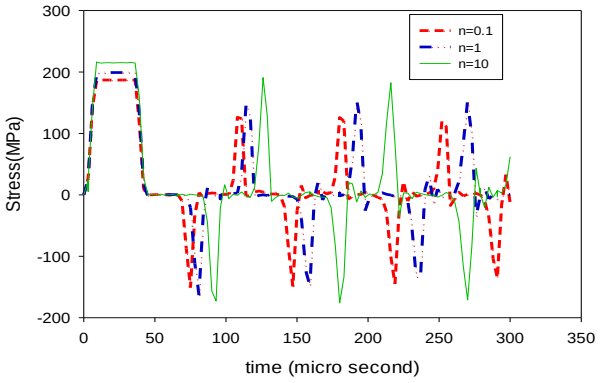

(a)

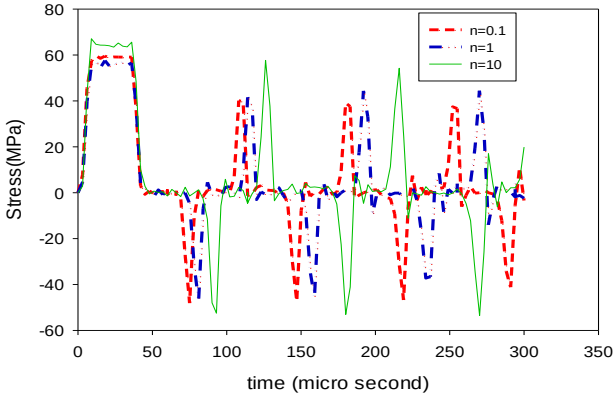

(b)

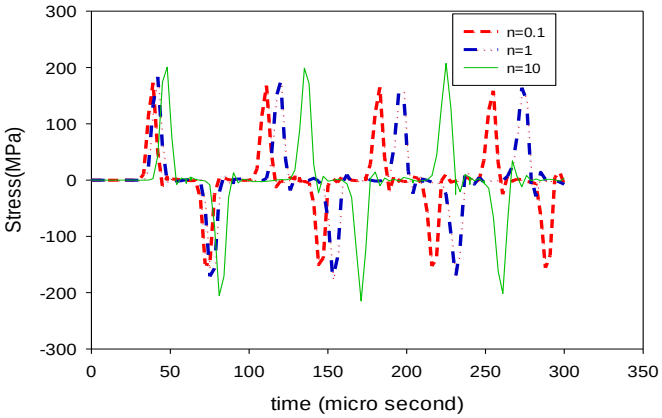

(c)

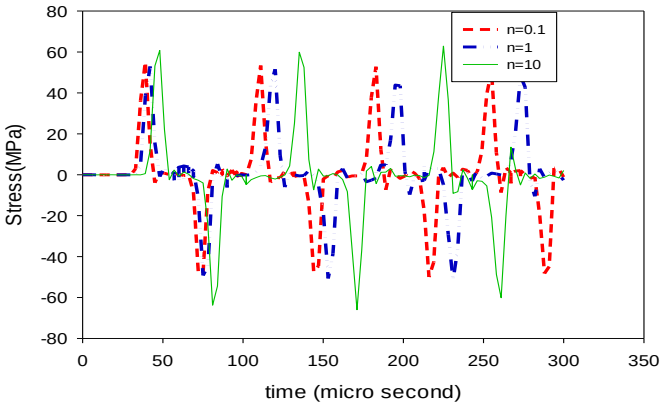

(d)

Figure 15. Distributions of the shear stress component $\sigma_{\theta z}$ In terms of time for the points (a)M,(b) N,(c) P and (d)Q for the compositional gradient exponents $n = 0.1,1,10$ for second specimen

In Fig. 15, it is observed that the maximum stresses occur at the points M and P and minimum stresses occur at points N and Q. In all of the points, the highest stress rate related to the $n=10$ and the lowest stress rate is related to the state $n=0.1$. Because the distribution of material properties in this case is one-dimensional, then the points that are on a radius, have approximately the same variation. By comparing Figures 12 and 15, it is shown that when the inner part of the functionally graded rod is Ti6A14V,the maximum stress occurred in mode $n=0.1$ and also when the inner part of the FG rod is Al2O3, the maximum stress occurred in mode $n=10$. In general, and in comparison, the maximum stresses of the points M and P in the second specimen and the maximum stresses of the N and Q points occurred in the first specimen. In the following, the strain variation charts are plotted in time for the second specimen for three modes $n=0.1,1,10$, separated by four points M, N, P and Q.

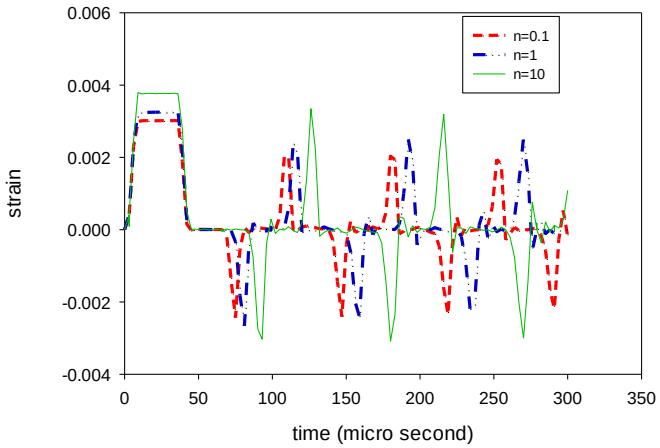

(a)

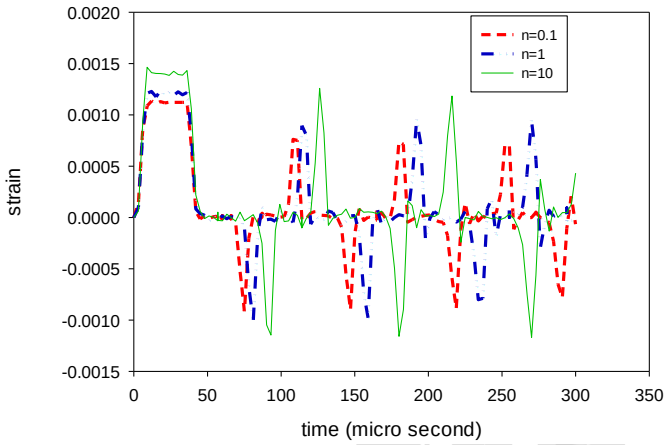

(b)

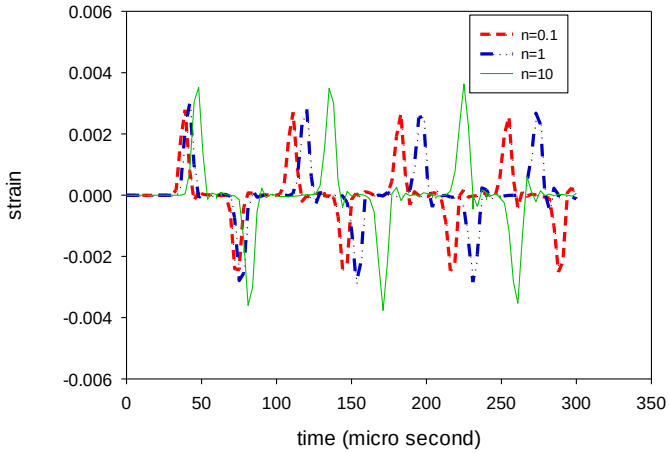

(c)

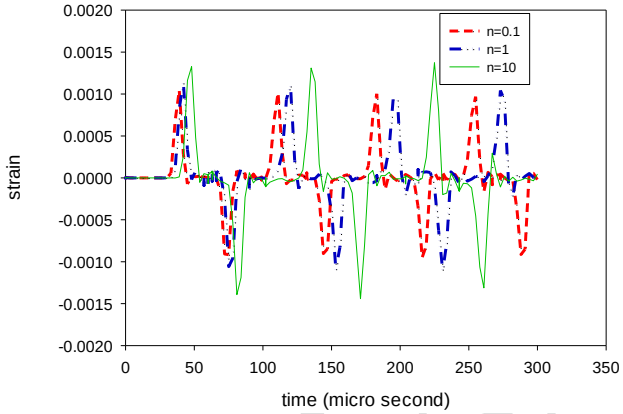

(d)

Figure 16. Distributions of the shear strain component $\varepsilon_{\theta z}$ In terms of time for the points (a)M,(b) N,(c) P and (d)Q for the compositional gradient exponents $n = 0.1,1,10$ for second specimen

Fig. 16 shows strain variations at points M, N, P, and Q in three modes. The maximum strain rate occurred at the points M and P. At all four points, the highest amount of variation in the state $n=10$ and the lowest amount of change occurred in state $n=0.1$. By comparing the strain charts in the first and second specimen, it is shown that in the first specimen, due to the fact that the inner part of the FG rod is composed of Ti6A14V, the maximum strain variation occurs in the $n=0.1$, and in the second specimen because The internal part of the FG rod made from Al2O3, the highest value of strain variation at all four points occurs in the $n=10$.

The displacement charts are plotted for $n = 0.1,1,10$ and the separation of points M, N, P, and Q in Figure 17.

In Fig. 17, it is expected that the maximum displacement occurs at the points M and N, and then in this case, the N and Q points have a lower displacement rate. By comparing the first and second specimen, it is shown that in the first specimen and at all four points, the highest amount of displacement occurs in the $n=10$. For the second specimen and at all four points, the highest rate of displacement occurred in the $n=0.1$.

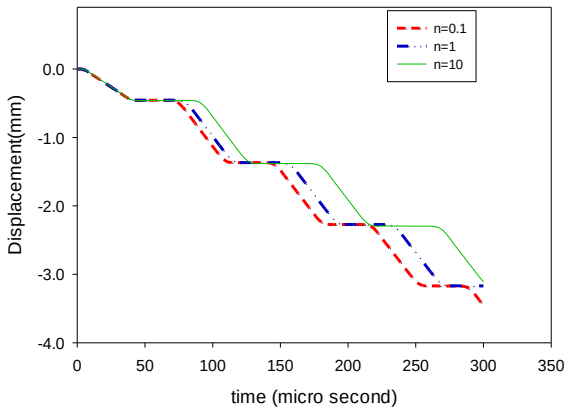

(a)

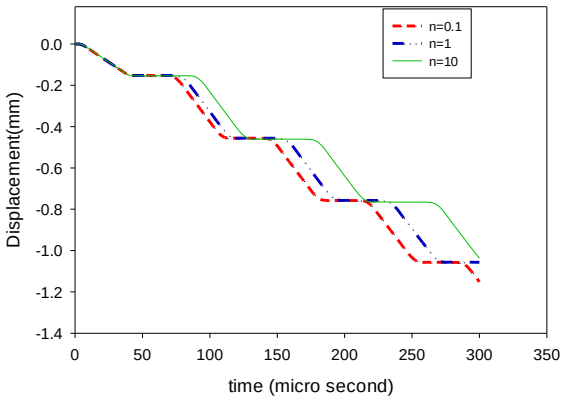

(b)

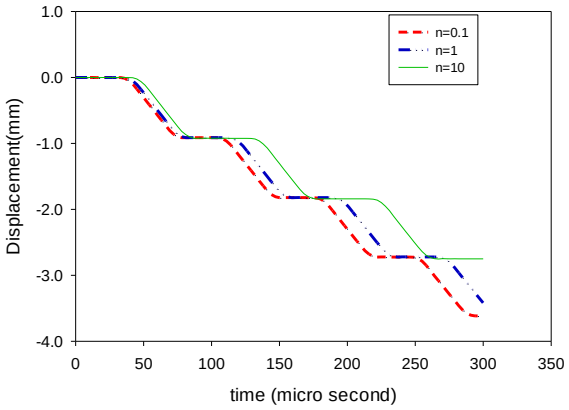

(c)

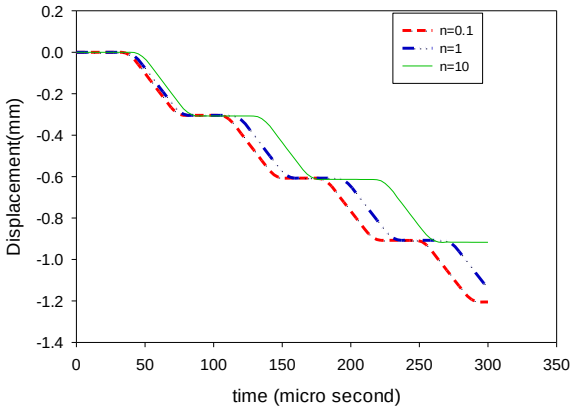

(d)

Figure 17. Distributions of the displacement component v In terms of time for the points (a) M,(b) N,(c) P and (d)Q for the compositional gradient exponents $n = 0.1,1,10$ for second specimen

5.3. State 3: FGM rod with two-dimensional distribution of materials

In this section, an FG rod with two-dimensional distribution of material has been studied. In state 3, the FG rod consists of four materials, two ceramic and two metal. Also, to study the effects of the properties of the ingredients, according to Fig. 5 and Table 8, four models of the FG rod are made with two-dimensional distribution of the materials mentioned. At first, the stress changes at the points M, N, P and Q were investigated and analyzed for the four mentioned models. Fig. 18, shows the variation chart of the stress rate in this state:

With respect to Fig. 18, it is shown that, as expected, the highest stresses were at points P and M and the lowest stresses occurred at points N and Q. Also, in each of the four-point, model 3 has the lowest value of stress. In points M and P, the highest stress is related to the second model, at the N and Q points in this case, the highest stress is related to model 4. The remarkable point in this case is that, unlike previous states, because in this case the distribution of properties of materials is in two dimensions, then the variation of stress in points that are located on a radius is not the same (points M and P and points N and Q).

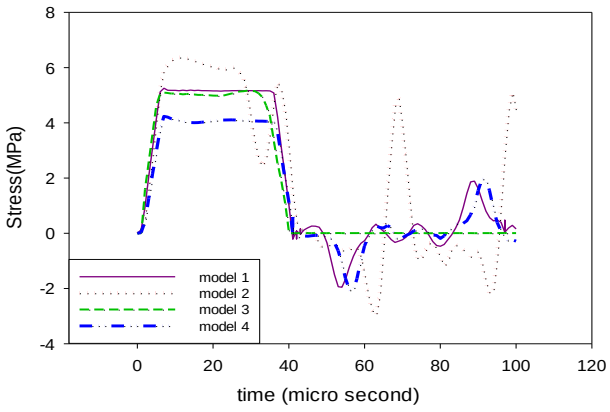

(a)

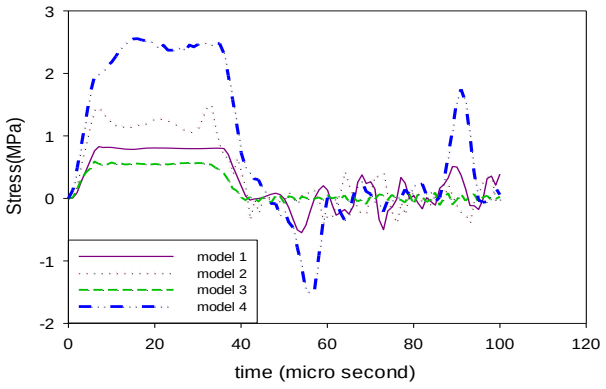

(b)

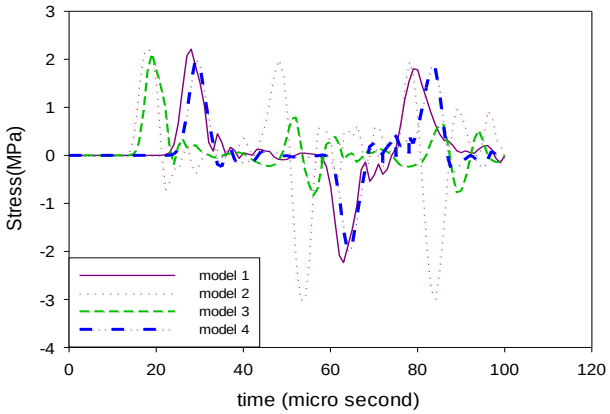

(c)

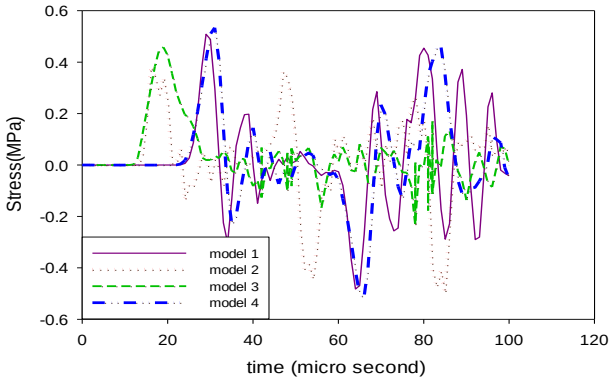

(d)

Figure 18. Distributions of the shear stress component $\sigma_{\theta z}$ In terms of time for the points (a) M, (b) N, (c) P and (d)Q for four models in state 3

Then, we analyzed the charts of the strain variations in time for 4 models and in four points M, N, P and Q in Fig. 19.

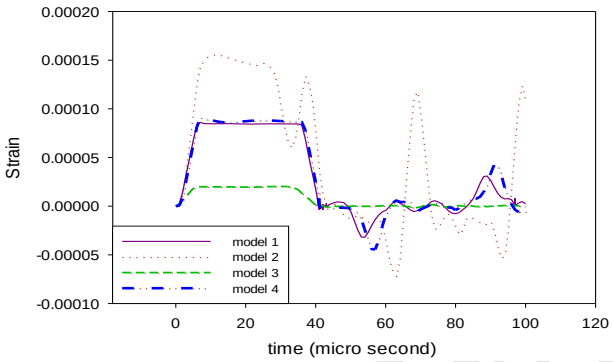

(a)

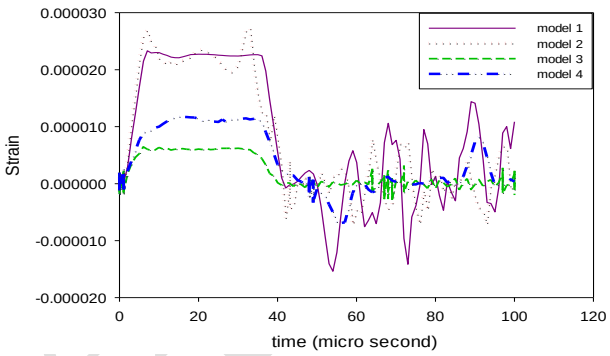

(b)

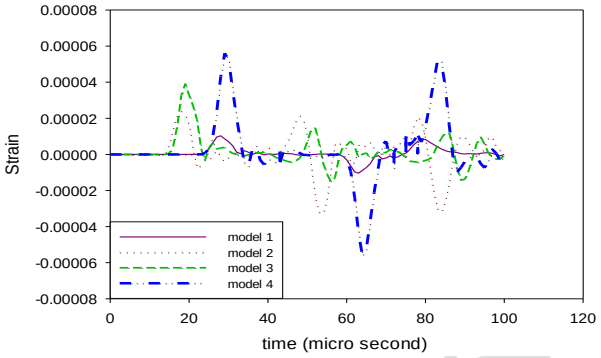

(c)

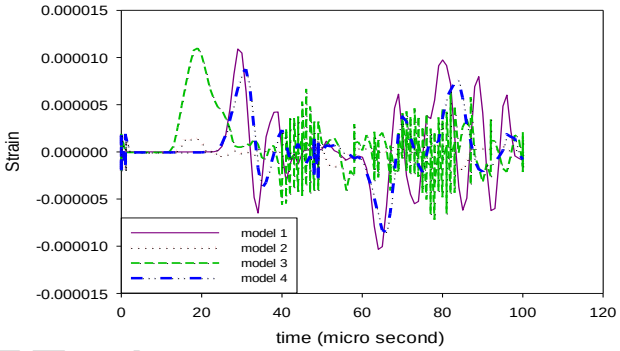

(d)

Figure 19. Distributions of the shear strain component $\varepsilon_{\theta z}$ In terms of time for the points (a)M, (b) N, (c) P and (d)Q for four models in state 3

In Fig. 19, we can say that the maximum strain value in this case is at the point M and in the model 2. Also, the lowest strain rate at all four points occurred in model 3. In this case, as the distribution of properties of materials is in two dimensions, so the amount of strain variation in the points on a radius is not the same and at each point of the FG rod the value of strain is different from the other points. To investigate the displacement of state 3, it is important to note that, since the torsion of the wave in the FG rod is discussed, then only the displacement in the direction v is non-zero.

In the following, the displacement charts are drawn in this state and separated by the points M, N, P and Q.

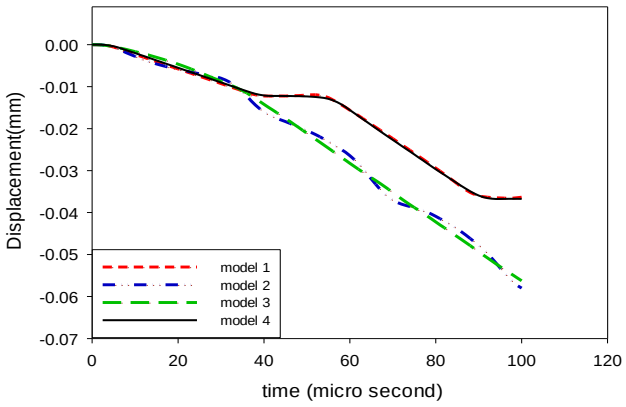

(a)

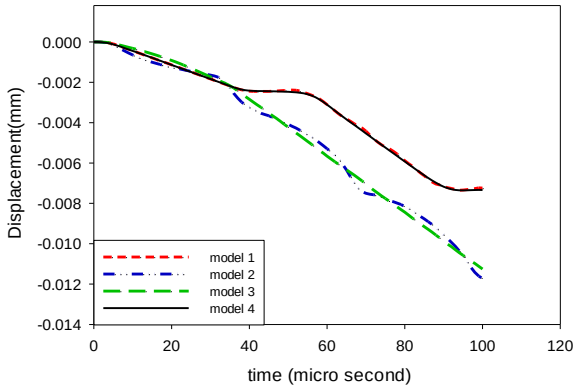

(b)

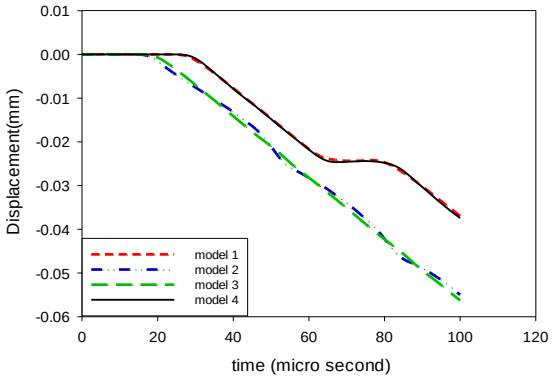

(c)

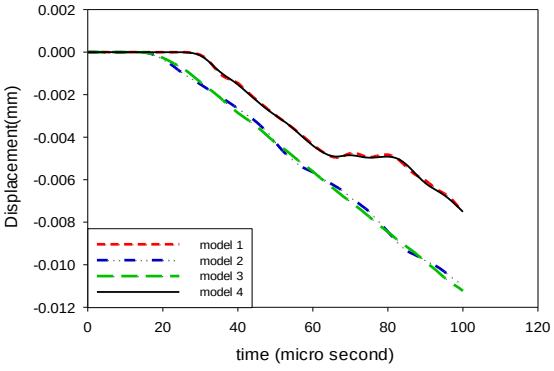

(d)

Figure 20. Distributions of the displacement component v In terms of time for the points (a)M, (b) N, (c) P and (d)Q for four models in state 3

In this case, the maximum displacement is observed at two points M and P. Also, according to Fig. 20, it is clear that in all four points, the displacement rate is approximately equal in two models, 2 and 3, and two models 1 and 4, respectively. The other point is that in intervals the same time, the displacement rate in models 1 and 4 is smaller than 2 and 3.

6. Boundary condition effects

In a new mode and considering the two-dimensional functionally graded rod, a new boundary condition is considered as a clamped, and stress, strain, and displacement diagrams for the four hypothesized points (M, N, P, Q) are plotted and analyzed. All details of the FG rod except boundary conditions are considered like state 3.

In Fig. 21 and in M and Q points, the most variation in stress is related to model 2. At the point N, the maximum stress has occurred in model 4. Also, at point P, the highest stress is for model 1. By comparing the four points in this case, it is determined that the highest stress level occurred at the point P and in the model 1. Also, due to the fact that the points P and Q are considered at the end of the FG rod, the stress wave has reached these points with a little delay. Comparing the four models for these two points, it is evident that in models 2 and 3, the wave has reached these points sooner.

In this case, the boundary condition is considered as a clamped and the strain-time charts are plotted for 4 points. According to the Fig. 22, it is clear that, in the points M and N, the highest strain rate is related to model 2. It is noteworthy that while the model 3 at the beginning of the rod (points M and N) has the lowest strain rate, but it has the maximum value of strain at the end of the rod (points P and Q).

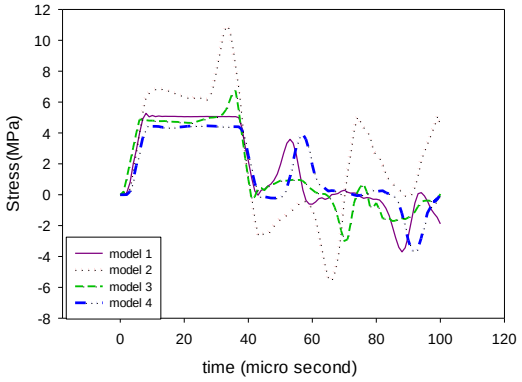

(a)

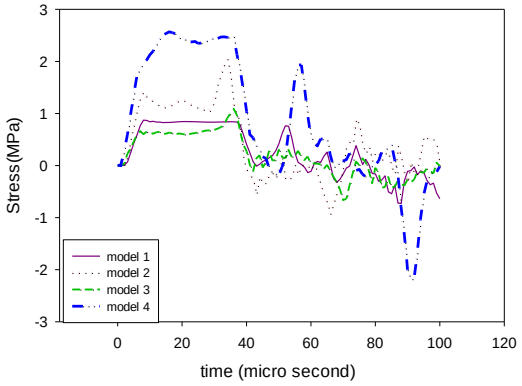

(b)

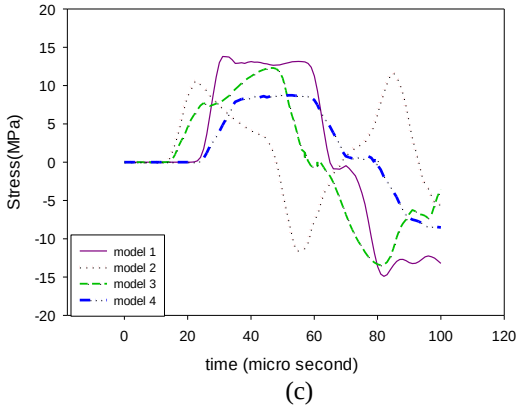

(c)

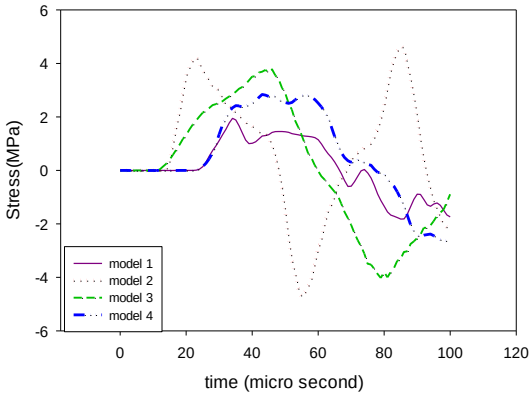

(d)

Figure 21. Distributions of the shear stress component $\sigma_{\theta z}$ in terms of time for the points (a) M, (b) N, (c) P and (d)Q for four models in mode clamped boundary condition

Fig. 23 is related to displacement-time charts for the points M, N, P and Q. with respect to this figure, it can be seen that the smallest initial peak in the M, N, and Q points is related to model 2. At the point P, the smallest initial peak can be seen in model 1. Also, given that the points P and Q, are at the end of the FG rod, So the displacement of these two points began with a slight delay. During this period, the greatest amount of displacement belongs to the point M and the least amount of displacement belongs to the point of Q.

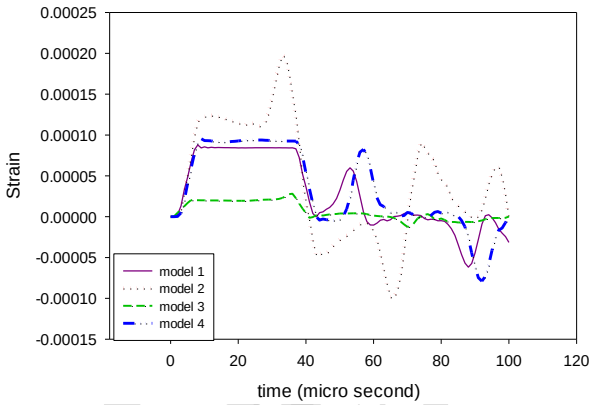

(a)

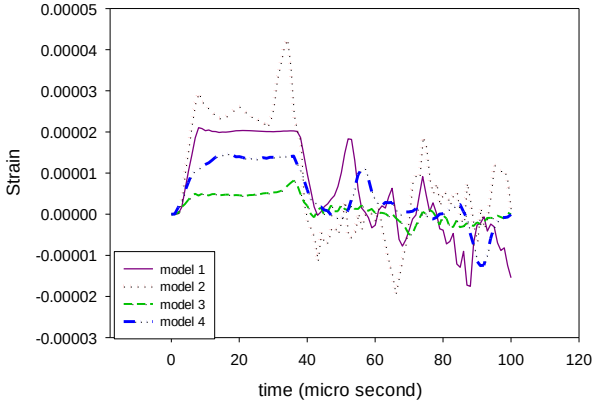

(b)

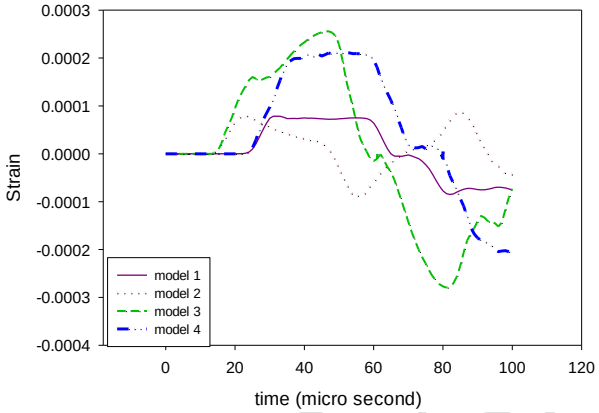

(c)

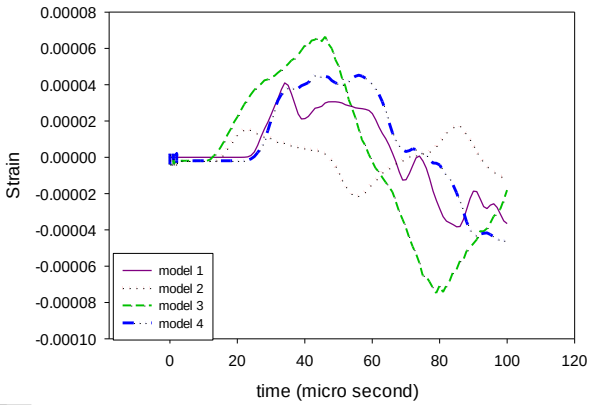

(d)

Figure 22. Distributions of the shear strain component $\varepsilon_{\theta z}$ in terms of time for the points (a)M, (b) N, (c) P and (d)Q for four models in mode clamped boundary condition

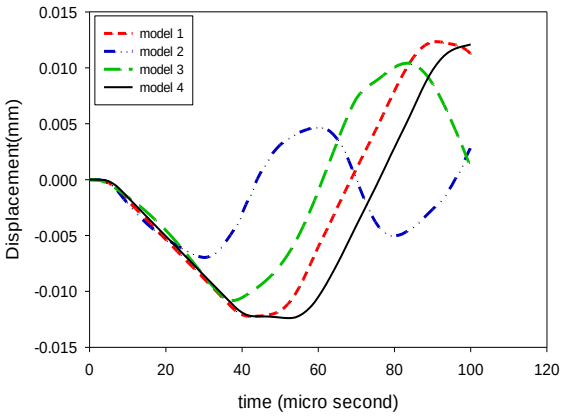

(a)

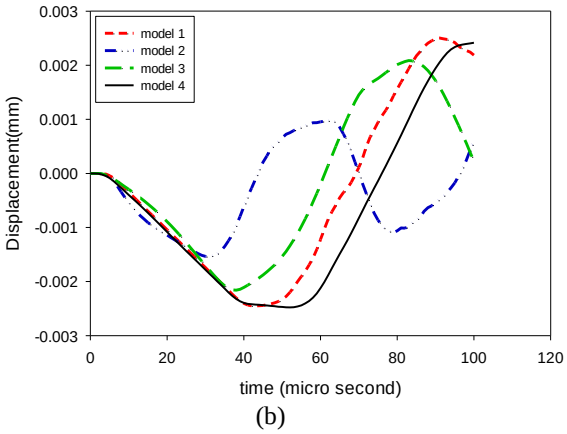

(b)

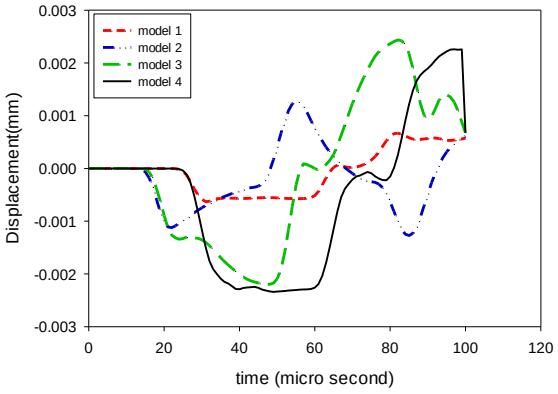

(c)

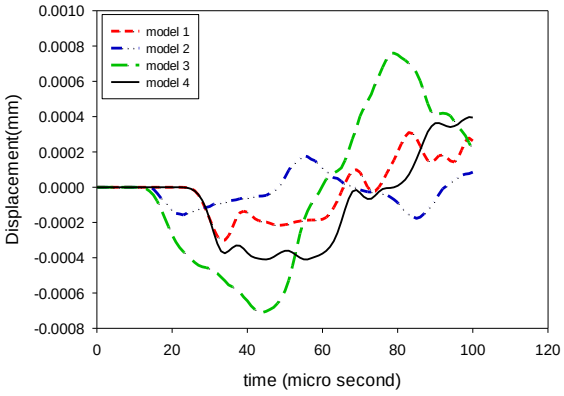

(d)

Figure 23. Distributions of the displacement component v in terms of time for the points (a)M, (b) N, (c) P and (d)Q for four models in mode clamped boundary condition

7. Cutoff frequency

To investigate the cutoff frequency in wave propagation, firstly, the ratio of stress in rode to the internal stress are calculated that is called gain. The amount of gain is showed in Fig. 24 for first state of isotropic rod.

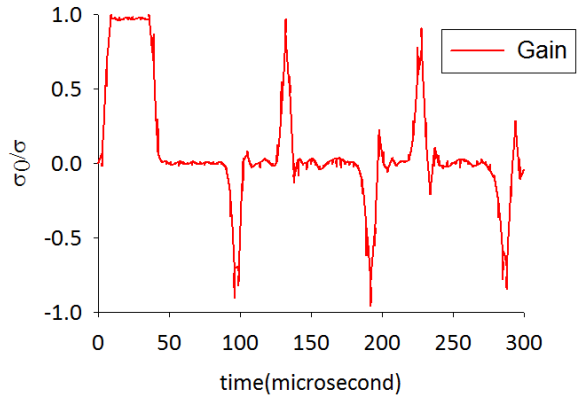

Figure 24. The gain of stress

By using of discrete Fourier transform in MATLAB, the frequency response of the above chart is calculated. Also, to compare the amount of frequencies with -3db that is the criterion of cutoff frequency, the vertical axis is converted to db. This chart is showed in Fig 25.

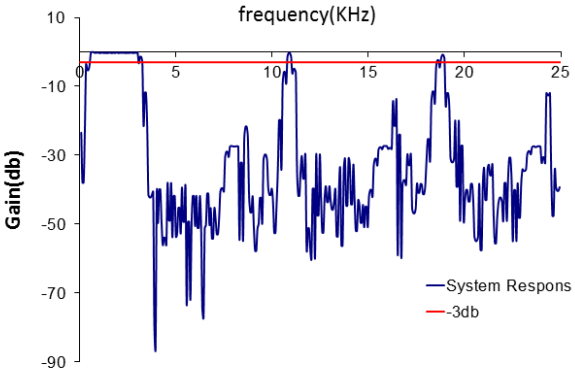

Figure 25. Frequency response of the stress wave propagation

As shown in this fig, the main lower cutoff frequency happens in 500 KHz and main upper cutoff frequency happens in 3241 KHz. Another cutoff frequency is occurred in 10875 and 18785 KHz.

For different states that mentioned later for material distribution in 1D and 2D, the cutoff frequency is calculated that the results are showed in Table 9.

Table 9. cut off frequency

FGM distribution			Lower cutoff frequency (KHz)	Higher cutoff frequency (KHz)
1D	Specimen1	n=1	478	3500
	Specimen1	n=0.1	491	3980
	Specimen1	n=10	430	3290
	Specimen2	n=1	449	4002
	Specimen2	n=0.1	509	4190
	Specimen2	n=10	512	3220
2D	Model 1		388	4220
	Model 2		441	4800
	Model 3		509	6930
	Model 4		498	3180

The results show that the lower cutoff frequency changes are neglectable but upper cutoff frequency directly depended to material properties. The compression of this results with mechanical properties of material, it can be understanding that density is more effective than other properties such as elastic module and Poisson ratio in cutoff frequency. With increasing density, the higher cutoff frequency is reduced and vice versa. Maybe it can be explained by inertia effects.

8. Conclusion

In this research, the propagation of torsional wave in the rod made of FGM materials has been investigated. The wave is considered to be a pulse, and it is applied to the desired rod within 40 microseconds. The method used to solve the torsional wave equations in this study is the finite difference method. The FGM materials used in this study are two types of ceramics and two types of metal. In the numerical result chapter of this study, torsional wave equations for an isotropic rod were initially solved and validated. Then, the equations are solved in three different states for the FG rod and discussed on the related charts. In a state with a one-dimensional distribution of properties, the equations for three different volume fractions are solved. In the state with the distribution of two-dimensional distribution of properties, four different models were made and the torsional equations for all the models were solved.

References

[1] L. Pochhamer, Uber die Fortpflanzzungsgeshwindigkeiten kleiner Schwingungen in einem unbergrenzten isotropen Kreiscylinder, *Zeitschrift fur Mathematik.*, Vol. 81, pp. 324, 1876.

[2] C. Chree, The equations of an isotropic elastic solid in polar and cylindrical co-ordinates their solution and application, *Transactions of the Cambridge Philosophical Society*, Vol. 14, pp. 250, 1889.

[3] A. E. H. Love, 1906, *A treatise on the mathematical theory of elasticity*, at the University Press,

[4] H.-S. Shen, 2016, *Functionally graded materials: nonlinear analysis of plates and shells*, CRC press,

[5] A. Berezovski, J. Engelbrecht, G. A. Maugin, Numerical simulation of two-dimensional wave propagation in functionally graded materials, *European Journal of Mechanics-A/Solids*, Vol. 22, No. 2, pp. 257-265, 2003.

[6] R. M. Mahamood, E. T. Akinlabi, M. Shukla, S. Pityana, Functionally graded material: an overview, 2012.

[7] M. Z. Nejad, A. Hadi, A. Rastgoo, Buckling analysis of arbitrary two-directional functionally graded Euler–Bernoulli nano-beams based on nonlocal elasticity theory, *International Journal of Engineering Science*, Vol. 103, pp. 1-10, 2016.

[8] A. Daneshmehr, A. Rajabpoor, A. Hadi, Size dependent free vibration analysis of nanoplates made of functionally graded materials based on nonlocal elasticity theory with high order theories, *International Journal of Engineering Science*, Vol. 95, pp. 23-35, 2015.

[9] M. Z. Nejad, A. Hadi, Non-local analysis of free vibration of bi-directional functionally graded Euler–Bernoulli nano-beams, *International Journal of Engineering Science*, Vol. 105, pp. 1-11, 2016.

[10] M. Z. Nejad, A. Hadi, A. Farajpour, Consistent couple-stress theory for free vibration analysis of Euler-Bernoulli nano-beams made of arbitrary bi-directional functionally graded materials, *Structural Engineering and Mechanics*, Vol. 63, No. 2, pp. 161-169, 2017.

[11] A. Hadi, M. Z. Nejad, A. Rastgoo, M. Hosseini, Buckling analysis of FGM Euler-Bernoulli nano-beams with 3D-varying properties based on consistent couple-stress theory, *Steel and Composite Structures*, Vol. 26, No. 6, pp. 663-672, 2018.

[12] M. Hosseini, M. Shishesaz, A. Hadi, Thermoelastic analysis of rotating functionally graded micro/nanodisks of variable thickness, *Thin-Walled Structures*, Vol. 134, pp. 508-523, 2019.

[13] M. Zamani Nejad, A. Rastgoo, A. Hadi, Effect of exponentially-varying properties on displacements and stresses in pressurized functionally graded thick spherical shells with using iterative technique, *Journal of Solid Mechanics*, Vol. 6, No. 4, pp. 366-377, 2014.

[14] M. Shishesaz, M. Hosseini, K. N. Tahan, A. Hadi, Analysis of functionally graded nanodisks under thermoelastic loading based on the strain gradient theory, *Acta Mechanica*, Vol. 228, No. 12, pp. 4141-4168, 2017.

[15] A. Barati, M. M. Adeli, A. Hadi, Static torsion of bi-directional functionally graded microtube based on the couple stress theory under magnetic field, *International Journal of Applied Mechanics*, 2020.

[16] M. Z. Nejad, N. Alamzadeh, A. Hadi, Thermoelastoplastic analysis of FGM rotating thick cylindrical pressure vessels

in linear elastic-fully plastic condition, *Composites Part B: Engineering*, Vol. 154, pp. 410-422, 2018.

[17] R. Noroozi, A. Barati, A. Kazemi, S. Norouzi, A. Hadi, Torsional vibration analysis of bi-directional FG nano-cone with arbitrary cross-section based on nonlocal strain gradient elasticity, *Advances in Nano Research*, Vol. 8, No. 1, pp. 13-24, 2020.

[18] T.-C. Chiu, F. Erdogan, One-dimensional wave propagation in a functionally graded elastic medium, *Journal of Sound and Vibration*, Vol. 222, No. 3, pp. 453-487, 1999.

[19] S.-H. Chi, Y.-L. Chung, Mechanical behavior of functionally graded material plates under transverse load—Part I: Analysis, *International Journal of Solids and Structures*, Vol. 43, No. 13, pp. 3657-3674, 2006.

[20] S.-H. Chi, Y.-L. Chung, Mechanical behavior of functionally graded material plates under transverse load—Part II: Numerical results, *International Journal of Solids and Structures*, Vol. 43, No. 13, pp. 3675-3691, 2006.

[21] M. Dorduncu, M. K. Apalak, H. Cherukuri, Elastic wave propagation in functionally graded circular cylinders, *Composites Part B: Engineering*, Vol. 73, pp. 35-48, 2015.

[22] L. Elmaimouni, J. Lefebvre, V. Zhang, T. Gryba, Guided waves in radially graded cylinders: a polynomial approach, *Ndt & E International*, Vol. 38, No. 5, pp. 344-353, 2005.

[23] M. Dorduncu, M. K. Apalak, Stress wave propagation in adhesively bonded functionally graded circular cylinders, *Journal of Adhesion Science and Technology*, Vol. 30, No. 12, pp. 1281-1309, 2016.

[24] J. Vollmann, D. M. Profunser, J. Bryner, J. Dual, Elastodynamic wave propagation in graded materials: simulations, experiments, phenomena, and applications, *Ultrasonics*, Vol. 44, pp. e1215-e1221, 2006.

[25] D. Sun, S.-N. Luo, Wave propagation and transient response of a FGM plate under a point impact load based on higher-order shear deformation theory, *Composite Structures*, Vol. 93, No. 5, pp. 1474-1484, 2011.

[26] K. Asemi, M. Akhlaghi, M. Salehi, Dynamic analysis of thick short length FGM cylinders, *Meccanica*, Vol. 47, No. 6, pp. 1441-1453, 2012.

[27] M. Shakeri, M. Akhlaghi, S. Hoseini, Vibration and radial wave propagation velocity in functionally graded thick hollow cylinder, *Composite structures*, Vol. 76, No. 1-2, pp. 174-181, 2006.

[28] J. Yu, X. Yang, J. Lefebvre, C. Zhang, Wave propagation in graded rings with rectangular cross-sections, *Wave Motion*, Vol. 52, pp. 160-170, 2015.

[29] M. Asgari, Two dimensional functionally graded material finite thick hollow cylinder axisymmetric vibration mode shapes analysis based on exact elasticity theory, *Journal of Theoretical and Applied Mechanics*, Vol. 45, No. 2, pp. 3-20, 2015.

[30] M. Asgari, Material optimization of functionally graded heterogeneous cylinder for wave propagation, *Journal of Composite Materials*, Vol. 50, No. 25, pp. 3525-3528, 2016.

[31] H. R. Hamidzadeh, R. N. Jazar, 2010, *Vibrations of thick cylindrical structures*, Springer,

[32] S. Xie, K. Liu, Transient torsional wave propagation in a transversely isotropic tube, *Archive of Applied Mechanics*, Vol. 68, No. 9, pp. 589-596, 1998.

[33] H. Cherukuri, T. Shawki, A finite - difference scheme for elastic wave propagation in a circular disk, *The Journal of the Acoustical Society of America*, Vol. 100, No. 4, pp. 2139-2155, 1996.

[34] W. Johnson, 1983, *Impact strength of materials*,